

Article

Mineralogy, Geochemistry, and Age Constraints on the Axinite-Bearing Gukjeon Pb–Zn Skarn Deposit in the Miryang Area, South Korea

Namhoon Kim, Sang-Mo Koh *, Byoung-Woon You and Bum Han Lee

Convergence Research Center for Development of Mineral Resources (DMR), Korea Institute of Geoscience and Mineral Resources, Daejeon 34132, Korea; nhkim@kigam.re.kr (N.K.); ybw8217@kigam.re.kr (B.-W.Y.); leebh@kigam.re.kr (B.H.L.)

* Correspondence: kohsm@kigam.re.kr; Tel.: +82-42-868-3106

Abstract: The axinite-bearing Gukjeon Pb–Zn deposit is hosted by the limestone, a member of the Jeonggaksan Formation, which, in turn, forms the part of the Jusasan subgroup of the Yucheon Group in the Gyeongsang Basin in the southeastern part of the Korean Peninsula. In this study, we attempted to interpret the spatial and temporal relationships among geologic events, including the mineralization of this deposit. We constructed a new 3D orebody model and suggested a relationship between skarn alteration and related mineralization. Mineralization timing was constrained using SHRIMP zircon age dating results combined with boron geochemistry on coeval intrusive rocks. Skarn alterations are restrictively found in several horizons of the limestone formation. The major skarn minerals are garnet (grossular), pyroxene (hedenbergite), amphibole (actinolite and ferro-actinolite), axinite (tizenite and ferro-axinite), and epidote (clinozoisite and epidote). The three stages of pre-skarn, syn-skarn, and post-skarn alteration are recognized within the deposit. The syn-skarn alteration is characterized by prograde metasomatic pyroxene and garnet, and the retrograde metasomatic amphibole, axinite, and epidote. Major skarn sulfide minerals are sphalerite, chalcopyrite, galena, and pyrite, which were predominantly precipitated during the retrograde stage and formed amphibole and axinite skarns. The skarn orebodies seem to be disc- or flat-shaped with a convex form at the central part of the orebodies. The vertical ascending and horizontal infiltration of boron-rich hydrothermal fluid probably controlled the geometry of the orebodies. Considering the whole-rock major, trace, and boron geochemical and geochronological results, the timing of Pb–Zn mineralization can be tightly constrained between the emplacement of boron-poor intrusion (fine-grained granodiorite, 82.8 Ma) and boron-rich intrusion (porphyritic andesite in Beomdori andesitic rocks, 83.8 Ma) in a back-arc basin setting. The boron for mineralization was sourced from late Cretaceous (Campanian), subduction-related magmatic rocks along the margin of the Pacific plate.

Keywords: axinite; Pb–Zn skarn; SHRIMP zircon U-Pb; Gyeongsang Basin; South Korea



Citation: Kim, N.; Koh, S.-M.; You, B.-W.; Lee, B.H. Mineralogy, Geochemistry, and Age Constraints on the Axinite-Bearing Gukjeon Pb–Zn Skarn Deposit in the Miryang Area, South Korea. *Minerals* **2021**, *11*, 619. <https://doi.org/10.3390/min11060619>

Academic Editor: George M. Gibson

Received: 10 May 2021

Accepted: 5 June 2021

Published: 9 June 2021

Publisher's Note: MDPI stays neutral with regard to jurisdictional claims in published maps and institutional affiliations.



Copyright: © 2021 by the authors. Licensee MDPI, Basel, Switzerland. This article is an open access article distributed under the terms and conditions of the Creative Commons Attribution (CC BY) license (<https://creativecommons.org/licenses/by/4.0/>).

1. Introduction

The Gukjeon Pb–Zn deposit is located within the Gyeongsang Basin, in the southeastern Korean Peninsula. Unlike the Great Limestone Series in the Taebaeksan Basin in the northeastern part of the Korean Peninsula where limestone-hosted skarn deposits are common, this sedimentary basin is much less widely mineralized. It contains a thick succession of non-marine sedimentary rocks such as conglomerate, sandstone, mudstone, and minor carbonate and volcanoclastic rocks [1]. Carbonate-hosted skarn ore deposits have rarely been found in the Gyeongsang Basin. The Gukjeon deposit was reported as a unique manto-type skarn deposit which was formed by skarnization and skarn mineralization of the limestone beds interbedded within the Late Cretaceous Jeonggaksan Formation in the Gyeongsang Basin [1].

Based on geological, mineralogical, and genetic research [2–6], three separate Pb–Zn orebodies have been identified in the limestone horizons of the Jeonggaksan sedimentary formation, and skarn alteration minerals (i.e., clinopyroxene, grossular, actinolite, axinite, and epidote) and skarn sulfide minerals (i.e., sphalerite and galena) have been identified [5,6]. However, the previous findings have not fully explained the exact occurrences and shapes of orebodies, nor the spatial and temporal relationships among the geologic events of sedimentation, volcanism, plutonic intrusion, and mineralization.

In this study, we attempted to identify an exact shape of orebodies and to construct a 3D model using geological information relating to the underground level, in order to more clearly represent the aspect of the mineralization caused in the limited horizons of the limestone formation. Zircon U–Pb geochronological and geochemical studies were carried out to interpret the spatial and temporal relationships among the geologic events, including the timing of mineralization.

This study is expected to provide the anatomical results for understanding the geological environment forming the Gukjeon Pb–Zn skarn deposit and for correlating the geological events of the Yucheon sub-basin (as well as the Gyeongsang Basin) in the southeastern part of the Korean Peninsula.

2. Regional Geology

The Gyeongsang Basin is tectonically subdivided into the Silla sub-basin, Yucheon sub-basin, and Yeongyang sub-basin from south to north (Figure 1). The Nagdong trough is bounded to the west from these three sub-basins. All of these tectonic provinces were formed in a large pull-apart basin within the back-arc environment related to the subduction of the Pacific plate (Figure 1) [7]. The study area, i.e., the Gukjeon Pb–Zn deposit, is located in the Miryang Block in the central part of the Yucheon sub-basin of the southern part of the Gyeongsang Basin (Figure 1).

The Gyeongsang Basin comprises the mainly sedimentary Shindong Group, volcanogenic Hayang Group, and volcanic Yucheon Group (Figure 1). About six hundred hydrothermal deposits, such as Au–Ag, Cu, Pb–Zn, and clay deposits, occur in this basin. The mineralization, showing progressive episodes from west to east within the Gyeongsang Basin, has been genetically associated with successive volcanism–plutonism–hydrothermal activities due to the subduction of the Pacific and Kula plates during the Late Cretaceous to the Early Tertiary (i.e., 100 to 60 Ma) [8].

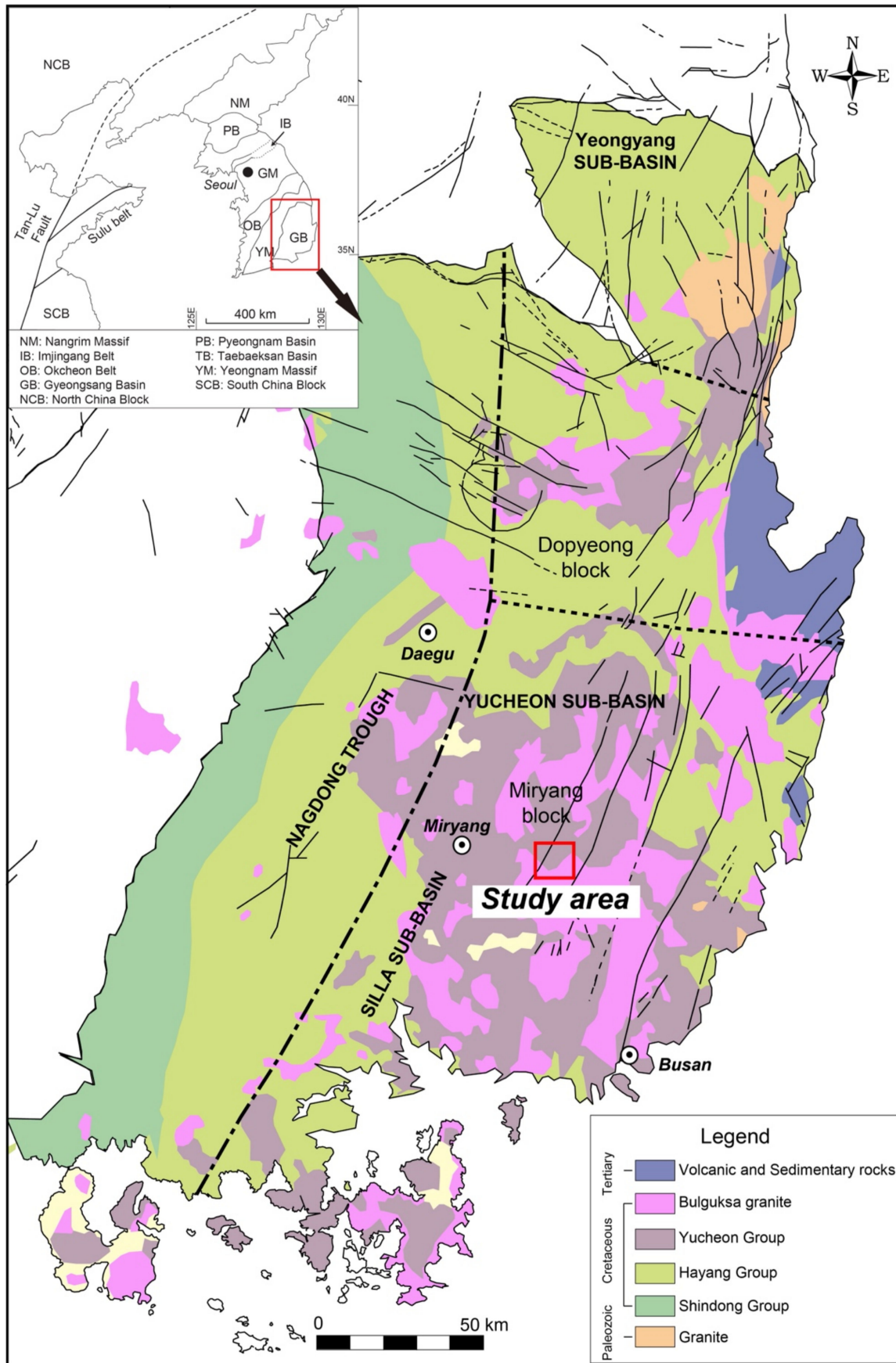


Figure 1. Geologic map of the Gyeongsang Basin in South Korea and location of the study area (modified from [7–9]).

3. Local Geology

The study area mainly consists of the late Cretaceous Yucheon Group and Bulguksa intrusives. The Yucheon Group is divided into the Jusasan subgroup (Jusasan andesitic rocks) and the Unmunsa subgroup (Unmunsa rhyolitic rocks). The Jusasan subgroup comprises aphanitic andesite, Miryang andesite, the Jeonggaksan Formation, and Beomdori andesite. The Unmunsa subgroup contains rhyolitic ash flow tuff, dacite, and rhyolite. The Bulguksa intrusives consist of fine-grained granodiorite, Eonyang granite (biotite granite), quartz porphyry, and acidic dykes (Figure 2).

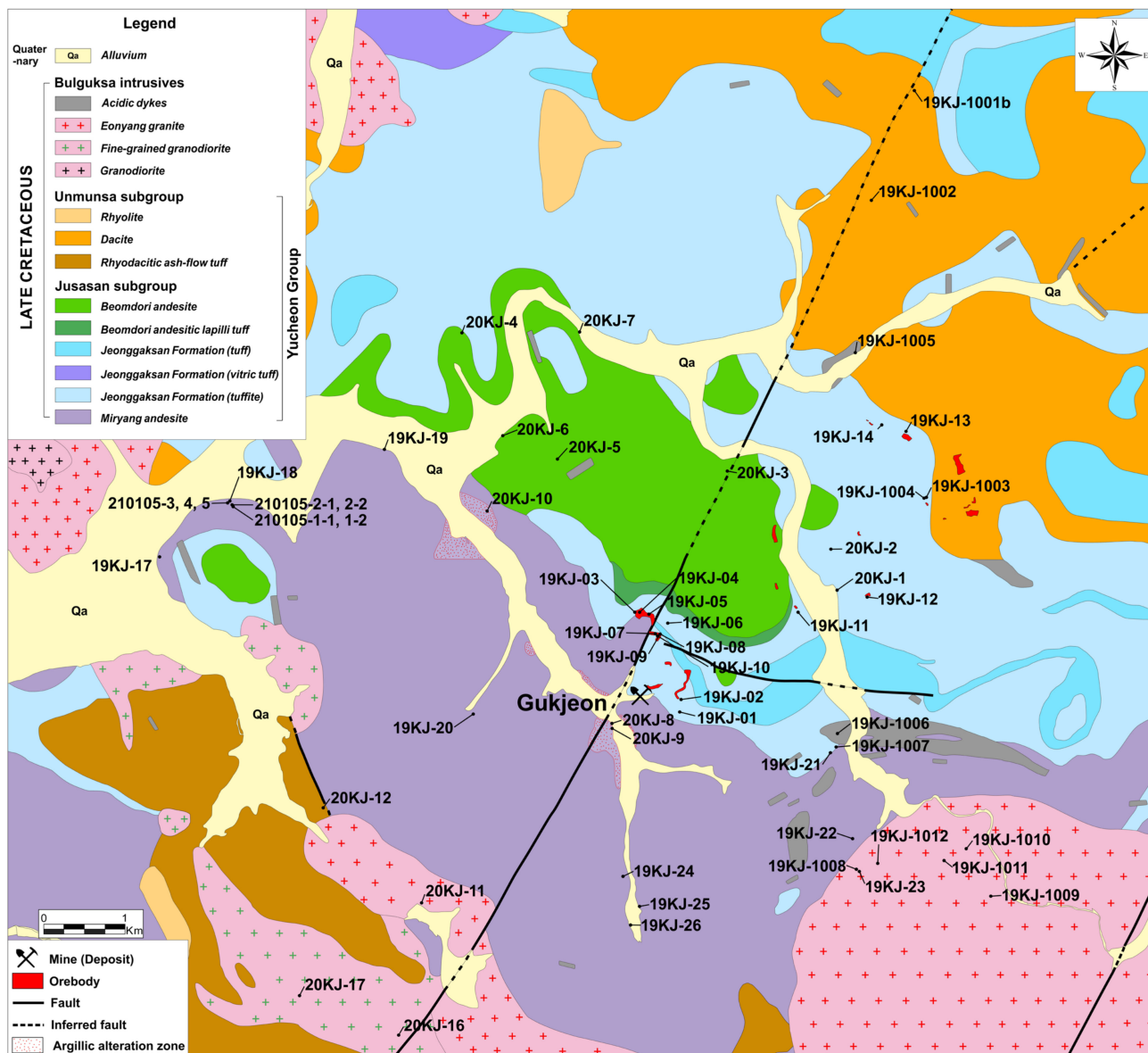


Figure 2. Geologic map and sample locality of the study area (modified from [10,11]).

The major Pb–Zn orebodies in the study area are mainly hosted by the limestone member of the Jeonggaksan Formation, and minor orebodies are distributed in the dacite of a member of the Unmunsa subgroup to the east of the Gukjeon Pb–Zn deposit (Figure 2). The deposit area is composed of hornfelsic siltstone and sandstone, andesitic tuff, andesite, skarns of the Jeonggaksan Formation, and the andesite and andesitic tuff of the Beomdori andesite. The mineralized interbedded limestones intermittently occur as several beds of 2–5 m in width and circa 50 m in length in the tuffaceous rocks of the Jeonggaksan Formation.

3.1. Miryang Andesite

Miryang andesite occurs throughout the southern part of the study area (Figure 2) and is mainly composed of andesitic lava and porphyritic andesite. Aphanitic andesite lava showing a typical trachytic flow structure consists of small plagioclase laths and a small amount of epidote (Figure S1A,B). These show gray, dark gray, and grayish-green colors and are carbonatized and epidotized, where epidotization is prominent near the pyrite veinlets (Figure S1A). Porphyritic andesite is characterized by plagioclase and pyroxene phenocrysts, and the plagioclase shows a compositional zonal variation (Figure S1C,D).

Andesitic rocks are the main host rocks of the Miryang pyrophyllite deposit far from the study area (about 14 km to the west). This deposit has been reported to be a hydrothermal pyrophyllite deposit, which was formed by Late Cretaceous post-volcanic activities in the Gyeongsang Basin [12]. The K–Ar age of sericite occurring in the deposit has been reported as 69.7 ± 2.1 Ma [13].

3.2. Jeonggaksan Formation

The 500 m thick Jeonggaksan Formation is the most widely exposed formation in the eastern and northern parts of the study area (Figure 2). This formation unconformably overlies the Miryang andesite (Figure S2A) and is underlain by the Beomdori andesite. It is mainly composed of green, gray, and purple tuffaceous shale, sandstone, conglomerate, and interbedded limestone, as well as intercalated andesitic crystal-lithic tuff (Figure S2C–F). Well-bedded tuffaceous sandstone and siltstone are the dominant components of this formation (Figure S2C). Andesitic tuff is also a main component of this formation, which is interbedded with tuffaceous sedimentary rock. This rock is a crystal lithic andesitic tuff with abundant feldspar crystals and essential andesitic rock fragments (Figure S2E,F). Some feldspars have been altered to epidote (Figure S2F). The limestone of this formation, with a thickness of several meters, is the host rock of the Pb–Zn skarn deposit (Figure S2B). Most limestones are skarnitized and the original composition is strongly changed, but the bedding is weakly preserved near the deposit.

3.3. Beomdori Andesite

The Beomdori andesite is distributed in the central part of the study area (Figure 2). This rock, which overlies the Jeonggaksan Formation and has an aphyric texture and dark greenish color, is mainly composed of lath-like plagioclase, chlorite, calcite, epidote, and subordinate with accessory minerals [10]. This andesite is interpreted as the latest volcanic product of the Jusasan subgroup in the study area. The rock near the deposit consists of aphanitic andesite lava and porphyritic andesite. The porphyritic andesite is composed of dominant phenocrysts of plagioclase and hedenbergite, and rarely orthoclase, (ferro-) actinolite, and cryptocrystalline groundmass (Figure S3A,B). Hedenbergite and (ferro-) actinolite phenocrysts have mostly been altered to chlorite.

3.4. Dacite

The dacite distributed in the northern part of the study area (Figure 2) has a prominent porphyritic texture (Figure S3C) with a cryptocrystalline groundmass. This rock is composed of dominant plagioclase phenocrysts, commonly of biotite, and rarely of orthoclase, and a microcrystalline groundmass of small plagioclase lath and quartz (Figure S3D).

3.5. Eonyang Granite (Bulguksa Intrusives)

The Eonyang granite distributed in the southern part of the study area (Figure 2) belongs to the Bulguksa intrusives. This rock has a typical granophyric texture with an intergrowth of alkali feldspar and vermicular quartz (Figure S3E,F). Small amounts of biotite and pyrite are associated with it. Most of the rocks in the study area belong to granophyre, which indicates the marginal facies of the stock of the Eonyang granite.

4. Methodology

The chemical compositions of major skarn minerals (i.e., pyroxene, garnet, amphibole, axinite, and epidote) were determined by using a field-emission electron probe micro-analyzer (JEOL JXA-8530F) at the core research facilities at the Gyeongsang National University, Jinju, Korea. Quantitative analyses were carried out under instrumental settings of a 15 kV accelerating voltage, a 10 nA beam current, a 5 μm beam diameter, and counting times of 20 s for peak measurements. The employed SPI standard materials were as follows: Si, diopside (SiO_2 54.98 wt.%); Al, pyrope garnet (Al_2O_3 21.50 wt.%); Fe, synthetic iron (FeO 99.99 wt.%); Mg, biotite (MgO 19.35 wt.%); Mn, spessartine garnet (MnO 41.02 wt.%), Ca, wollastonite (CaO 48.00 wt.%); Na, albite (Na_2O 11.48 wt.%); K, K-feldspar (K_2O 5.62 wt.%); Ti, sphene (TiO_2 37.81wt%); Cr, synthetic chromium (Cr_2O_3 99.99 wt.%).

The underground map was taken from a previous study [3]. We could only access level 0 in the Gukjeon deposit, as the other levels (1–9) were flooded and inaccessible. For level 0, we obtained 3D cloud point data using a 3D laser scanning system (Riegl VZ-400i, RIEGL Laser Measurement Systems GmbH, Riedenburgstraße, Austria) and reproduced the 3D underground mining model. The numerical data for the rest of the levels were obtained by digitizing from the 2D raster underground map. The final 3D geology and orebody geometry were made by merging the 3D scanned data for level 0 and digitized numerical data for levels 1–9.

The whole rock major and trace elements were analyzed on the molten bead by induced coupled plasma (ICP)–optical emission spectrometry and ICP–mass spectrometry at Activation Laboratory Ltd (Actlabs, Ancaster, ON, Canada) in Canada. Boron elements were analyzed by prompt-gamma neutron activation analysis using pulverized powder at Actlabs and the detection limit was 10 ppm.

Zircon separation was carried out according to the following procedure. Crushed rock powders smaller than 200 μm caused overflow of light mineral grains out of the beaker and magnetic minerals (e.g., magnetite, etc.) were removed by conventional magnetic separation, after which zircon grains were handpicked under a binocular microscope. The analytical points were decided after backscattered electron and cathodoluminescence (CL) imaging using a JEOL 6610LV (JEOL Ltd, Tokyo, Japan) scanning electron microscope at the Korea Basic Science Institute (KBSI). The SL13 (Sri Lankan Gem zircon) and FC1 (Duluth gabbroic anorthosite, 1099 Ma) [14] standard zircons were employed for U concentration (238 ppm) and U–Pb aging. The U–Th–Pb isotopic compositions were measured using the SHRIMP IIe/MC at KBSI. The analytical procedure of [15] was followed. Terra–Wasserburg diagrams and weighted mean age calculations were performed using Isoplot software (version 3.7–Berkeley Geochronology Center, CA, USA [16]). In this study, we used ^{208}Pb corrected U and Pb isotopic data for the Terra–Wasserburg diagrams and ^{207}Pb corrected $^{206}\text{Pb}/^{238}\text{U}$ ages for calculating the weighted mean ages.

5. Alteration

5.1. Pre-Skarn Alteration

Contact metamorphic alteration before the skarnization strongly affected the tuffaceous and sedimentary rocks of the Jeonggaksan Formation. In particular, argillaceous and arenaceous sedimentary rocks were completely altered to hornfels. Most the hornfelsic rocks are distributed near the skarn orebodies of the Gukjeon Pb–Zn deposit. They are commonly found within the skarn zone of the underground and outcrops. The dense and hard hornfelsic rocks are mainly composed of small crystalline quartz, plagioclase, muscovite, chloritized biotite, and calcite (Figure 3B). In addition, the matrix consists of very fine quartz and sericite. Despite the strong alteration, the original bedding and/or lamination of the host sedimentary rocks are well preserved in most areas (Figure 3A).

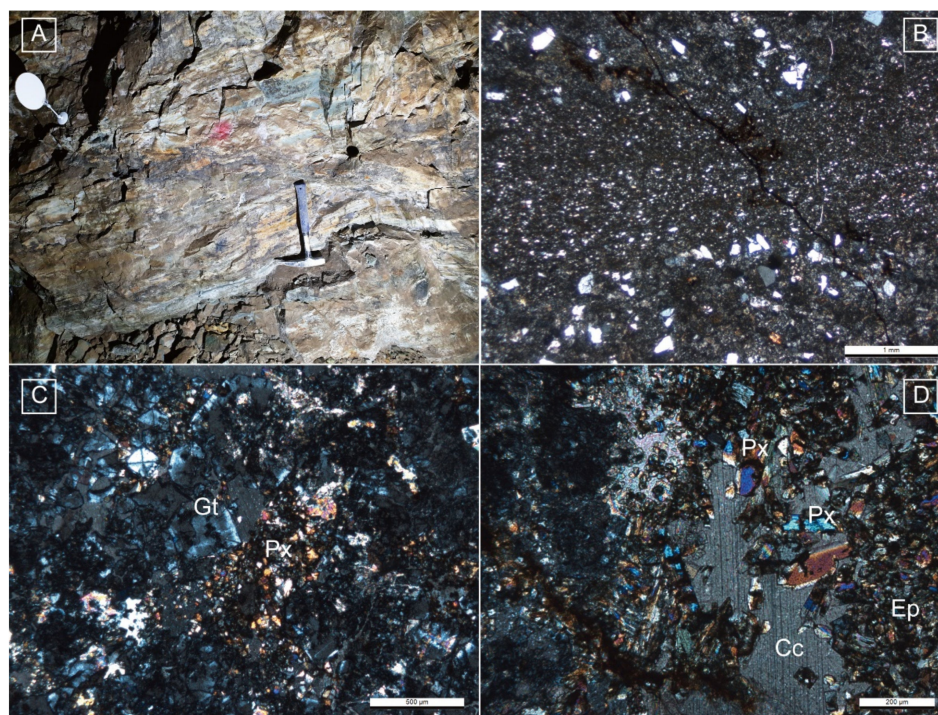


Figure 3. Hornfelsic laminated tuffaceous siltstone in the underground (A) and its microphotograph (B). Microphotographs of garnet skarn (C) and epidote skarn (D). (B–D) are under crossed nicols. (C) Small fragment pyroxene (Px) relics are replaced by garnet (Gt) in the garnet skarn (C). (D) Epidote (Ep) replaces calcite (Cc) and pyroxene (Px) in the pyroxene skarn (D).

5.2. Skarn Alteration

Skarn alteration of the Gukjeon Pb–Zn deposit is restricted to limestone interbedded with tuffaceous sedimentary rocks in the Jeonggaksan Formation. The representative skarn minerals are garnet, pyroxene, amphibole, axinite, and epidote. On the basis of optical microscope textural analyses, the skarn alteration can be divided into prograde and retrograde stages. The prograde stage is the metasomatic anhydrous stage. Garnet and pyroxene are formed in this stage and these commonly replaces the primary calcite and are replaced by the second stage retrograde phases, including amphibole, axinite and epidote, etc. during the following retrograde skarnization. The second stage is the retrograde hydrous stage. The most abundant skarn minerals of this stage are amphibole, axinite, and epidote. The detailed occurrences and geochemical characteristics of skarn minerals are as follows.

5.2.1. Pyroxene

Most pyroxenes occur as fragmented aggregates and discrete grains of small crystal relics in the skarn zone. They are replaced by anisotropic garnet (Figure 3C) and large bladed axinite or replace large crystals of calcite (Figure 3D). Judging from these replacement processes and occurrences, pyroxene seems to be the first prograde skarn mineral in the deposit. EPMA analytical results for pyroxenes at 19 points are shown in Table S1. Plotting to ternary diagrams (Mg–Ca–Fe²⁺) for the analytical results of pyroxenes, they were mostly classified as hedenbergite (Figure 4).

5.2.2. Garnet

Garnets are one of the most commonly occurring skarn minerals in the deposit. They are strongly fragmented and scattered as very small grains (Figure 5B). Generally, garnet replaces calcite and is replaced by epidote (Figure 5A,C,D) and amphibole. The garnet is associated with fragmented pyroxene aggregates and is abundant in the marginal zone of the Pb–Zn main orebody. Judging from these replacement processes and occurrences,

garnet is the second prograde skarn mineral (after pyroxene) in the deposit. EPMA analytical results for garnet at 13 points are shown in Table S2. Except for one sample, all of the analyzed garnets have a high grossular proportion (X_{Grs}) ranging from 78.45 to 83.90% and an andradite proportion (X_{And}) ranging from 6.28% to 18.80%. The garnet grains from sample 19KJU-4-1 have higher andradite proportions (81.86% and 90.67%) than the other samples and lower grossular proportions (6.17% and 12.75%). As shown in Figure 6, whole analyzed garnets are plotted in the field of skarns/low-grade metabasic rock/calc-silicate granulite (Figure 6).

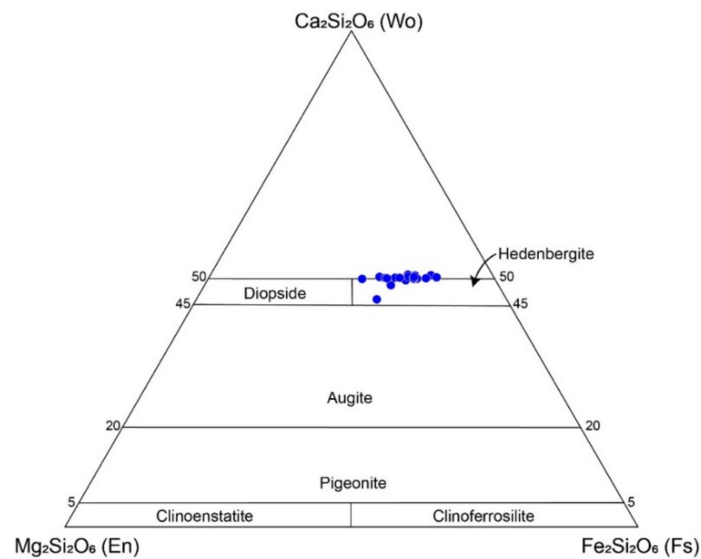


Figure 4. Ca–Mg–Fe clinopyroxene classification diagram after [17].

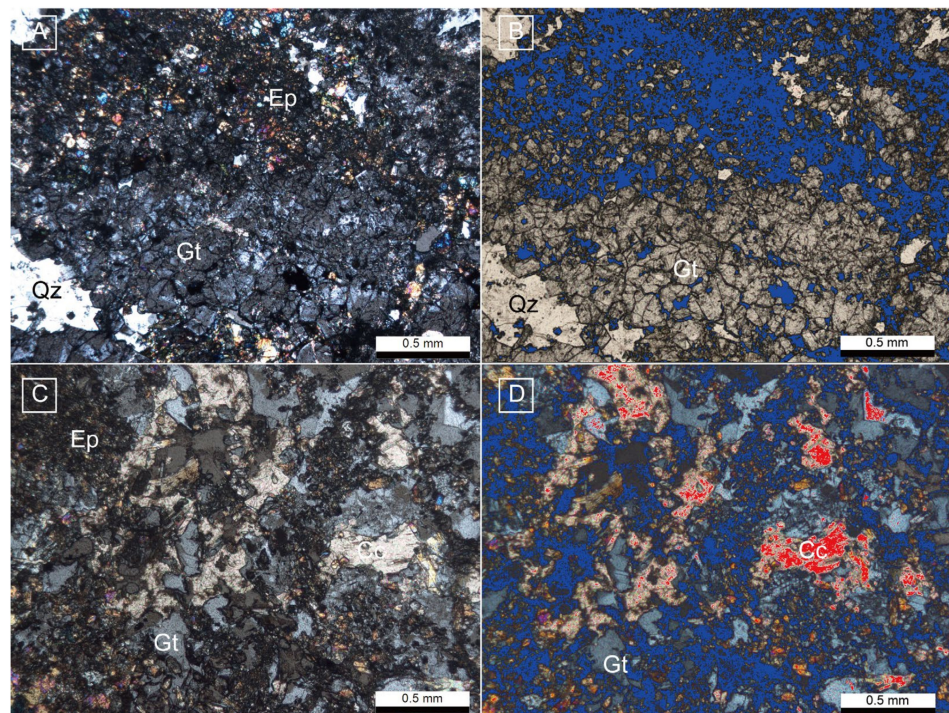


Figure 5. Microphotographs of the garnet skarn (A,C) are under crossed nicols; (B,D) are exposure-adjusted under open nicol and crossed nicol, respectively). (A,B) Large garnet crystal (Gt) is replaced by small epidote aggregate (Ep) and is strongly fragmented. (C,D) Garnet replaces calcite (Cc) and calcite remains after the replacement of garnet.

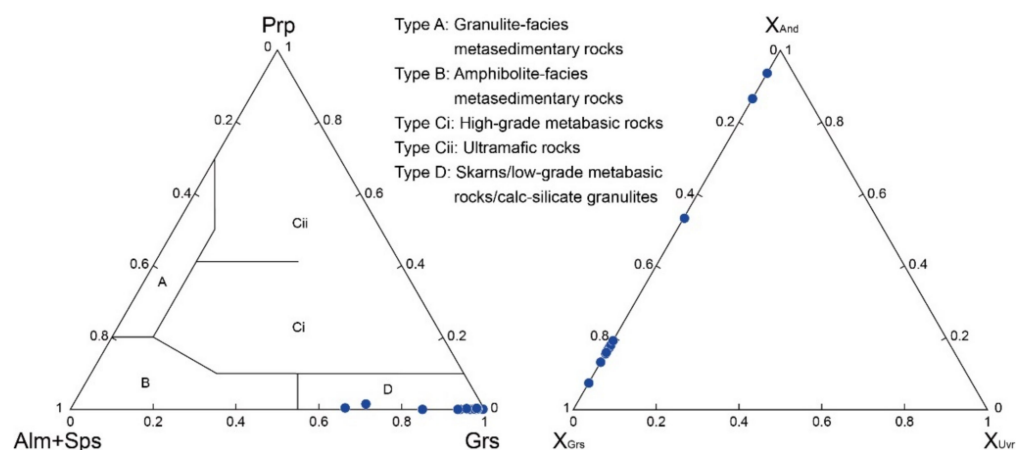


Figure 6. Garnet classification scheme of [18] (left) and $X_{\text{And}}-X_{\text{Grs}}-X_{\text{Uvr}}$ ternary diagram (right).

5.2.3. Amphibole

Amphibole is the most abundant retrograde skarn mineral in the deposit. It generally occurs as long prismatic, small, flat, and/or fibrous aggregates (Figure 7A,B). It overprints most of the primary minerals, such as calcite, and the prograde skarn minerals, such as pyroxene and garnet (Figure 7B,C). They are sometimes injected by axinite veinlets. Judging from these replacement processes and occurrences, amphibole is the first retrograde skarn mineral in the deposit. EPMA analytical results for amphibole at 11 points are shown in Table S3.

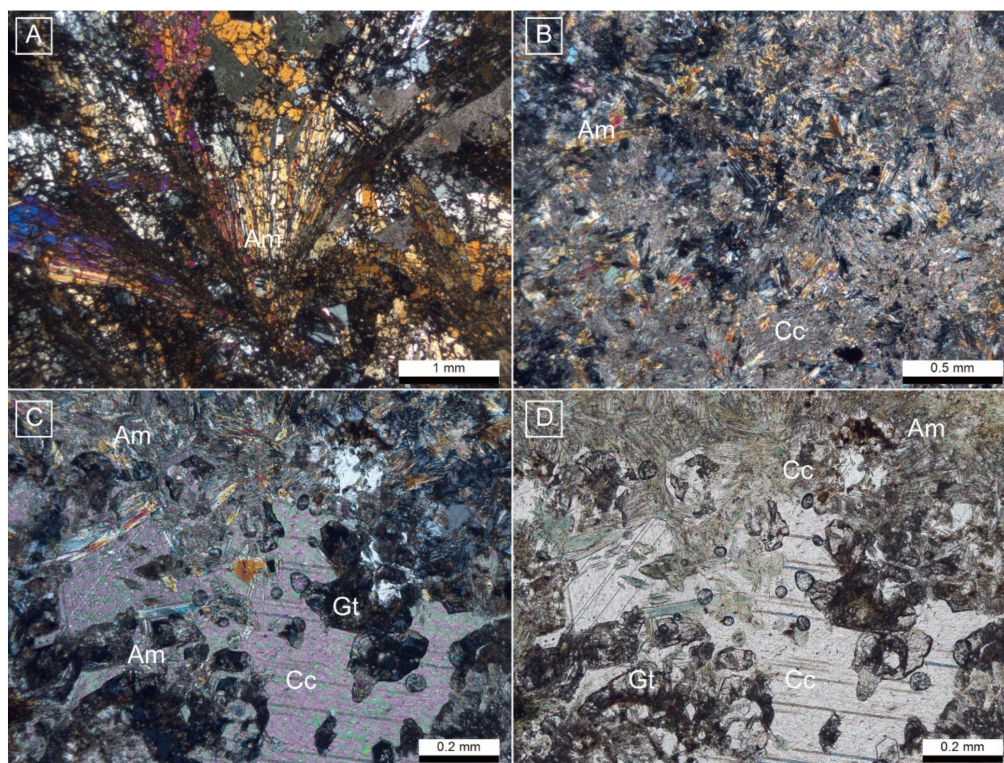


Figure 7. Microphotographs of amphibole skarn (A–C) are under crossed nicols; (D) is under open nicol. Amphibole (Am) occurs as a prismatic radial aggregate (A) and a fibrous aggregate (B). Fibrous amphibole aggregate overprints calcite (Cc) matrix and fragmented garnet (Gt).

Plotting to the discrimination diagram of amphibole, they are classified as actinolite and ferro-actinolite (Figure 8).

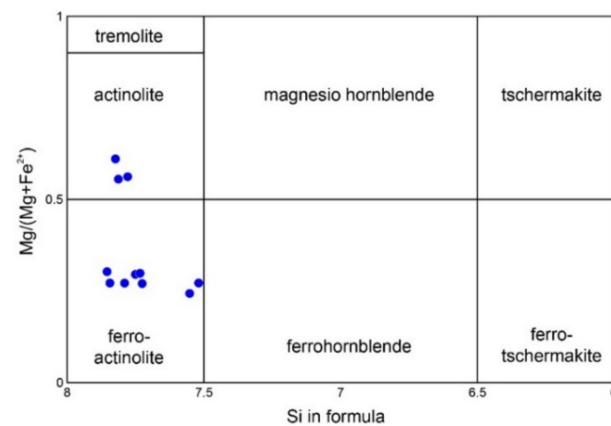


Figure 8. Classification of the calcic amphibole diagram after [19].

5.2.4. Axinite

Axinite is the most characteristic skarn mineral and occurs abundantly throughout the deposit. Axinites occur mostly as large crystals with a wedge or axe-head shape, or sometimes a fragmented irregular shape. They occur as cavity filling (Figure 9A) and veinlet (Figure 9B). Axinite replaces primary calcite and the retrograde skarn mineral, amphibole (Figure 9D), and is replaced by small grains of epidote (Figure 9B). Sometimes, axinite veinlets are injected into the amphibole skarn (Figure 9C,D). Judging from these replacement processes and occurrences, axinite is the second retrograde skarn mineral (after amphibole) in the deposit. EPMA analytical results for axinite at 10 points are shown in Table S4. Plotting to a discrimination diagram of axinite, they are classified as Mn- and Fe-rich tizenite and ferroaxinite (Figure 10).

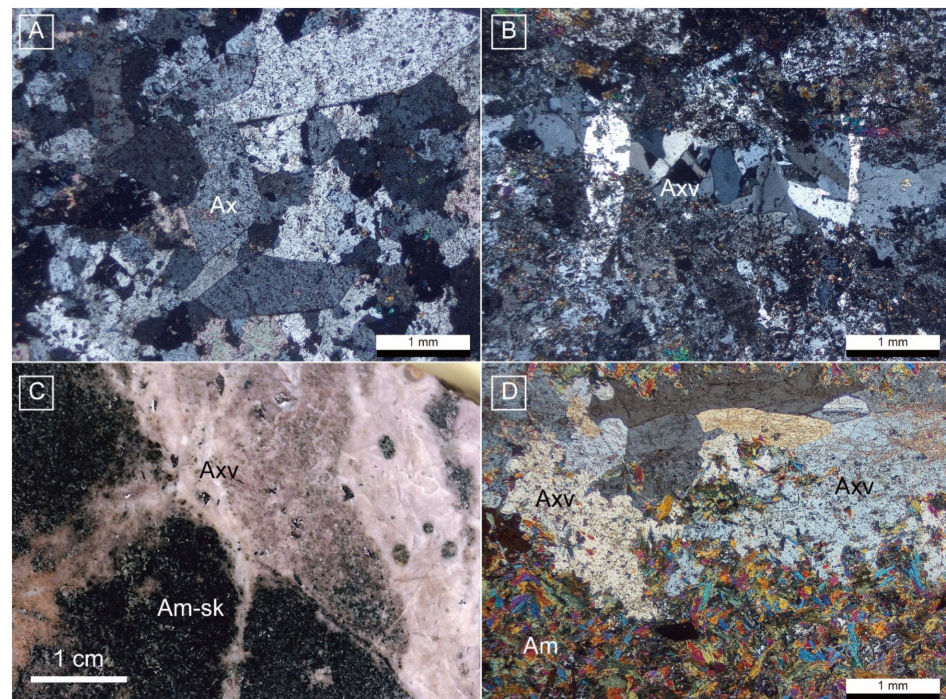


Figure 9. Microphotographs of axinite skarn (A,B,D) are under crossed nicols and (C) is rock slab. (A) Wedge and axe-head shaped axinite (Ax). (B) Axinite veinlet (Axx) and small grains of epidotes. (C,D) Axinite veinlet (Axx) is injected into the amphibole skarn (Am-sk).

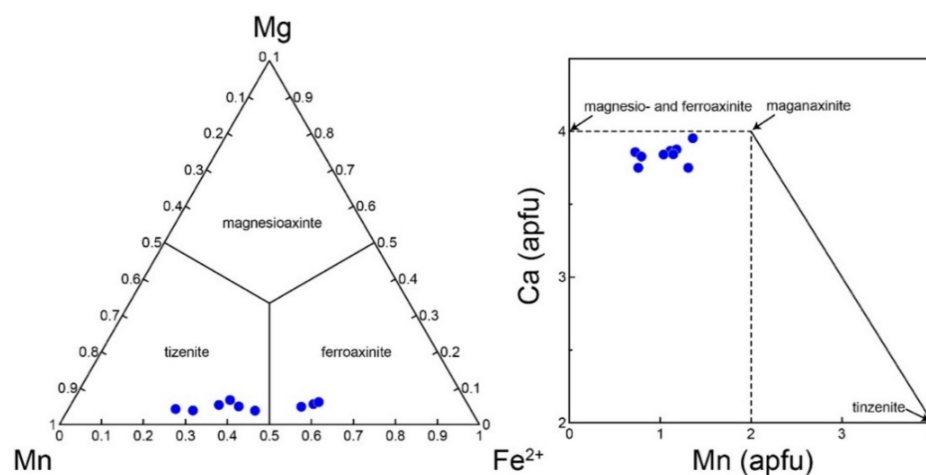


Figure 10. Chemical compositions of analyzed axinite after [20].

5.2.5. Epidote

Epidote is one of the most abundant skarn minerals in the deposit. It occurs as small to large lath forms and fills the matrix as small aggregates. It generally occurs as veinlets and has a layered form. Epidote commonly replaces the primary calcite (Figure 11A) and cross-cuts pre-existing skarn minerals such as pyroxene, garnet, amphibole, and axinite (Figure 11B–D). These replacement textures and occurrences indicate that the epidote is the final retrograde skarn mineral (after amphibole and axinite) in the deposit. EPMA analytical results for epidote at 32 points are shown in Table S5. Plotting to a discrimination diagram of epidote, they are classified as mostly epidote–clinzoisite (Figure 12).

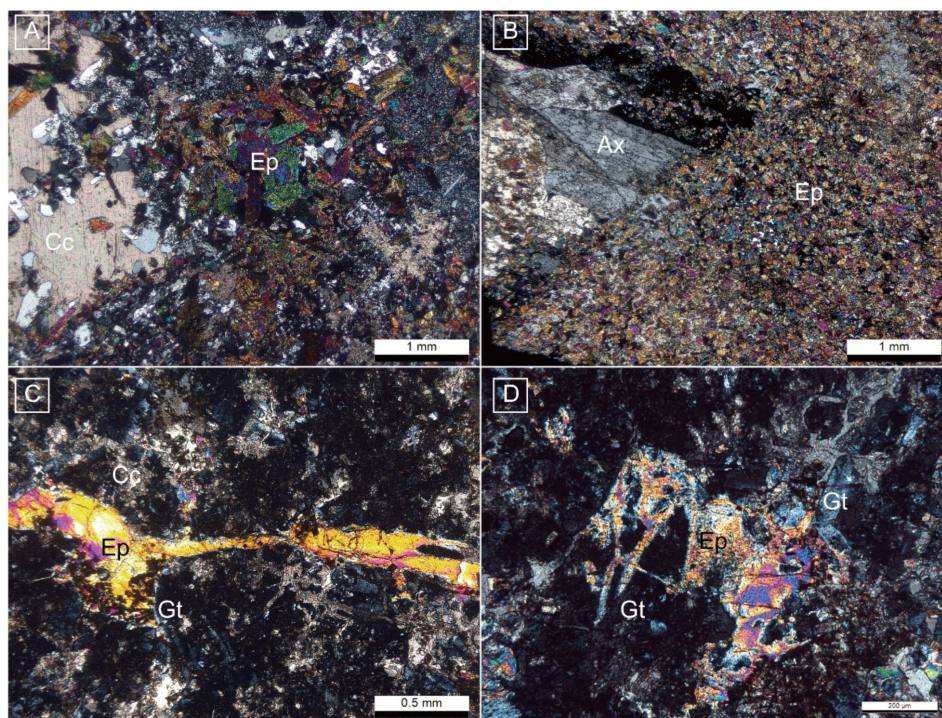


Figure 11. Microphotographs of the epidote skarn (A,B) and the garnet skarn (C,D). All the photos are under crossed nicols. (A) Thin and prismatic epidote (Ep) replaces calcite (Cc). (B) Small crystals of epidote aggregate (Ep) cross-cut axe-head shaped axinite (Ax). (C,D) Epidote (Ep) veinlet in the garnet skarn, composed mainly of garnet and calcite (Cc).

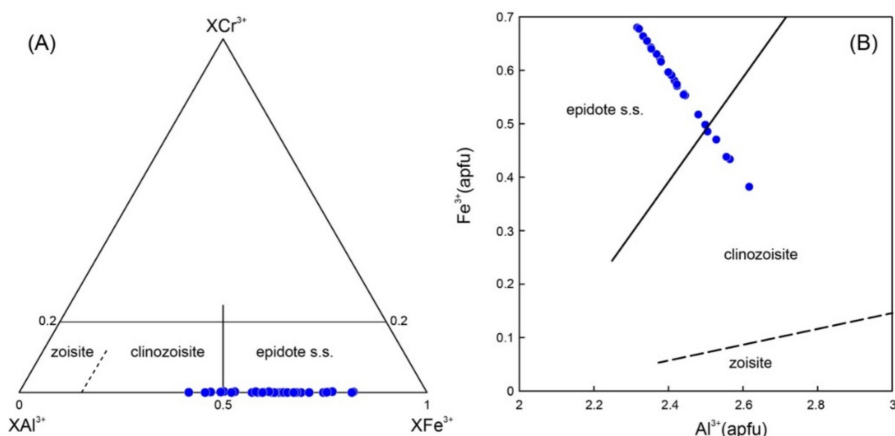


Figure 12. Epidote classification diagrams. Ternary diagram based on XAl^{3+} – XFe^{3+} – XCr^{3+} (adopted from [21]) (A); and Al^{3+} vs. Fe^{3+} diagram (B).

5.3. Post-Skarn Alteration

The post-skarn alterations of the deposit mostly consist of chloritization and silicification. Chloritization took place in favor of the fracture zone (Figure 13A) and in the selective layering (Figure 13B).

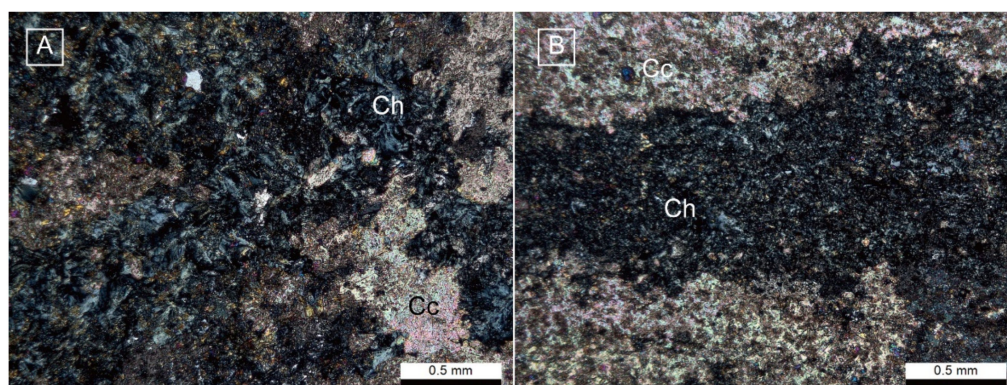
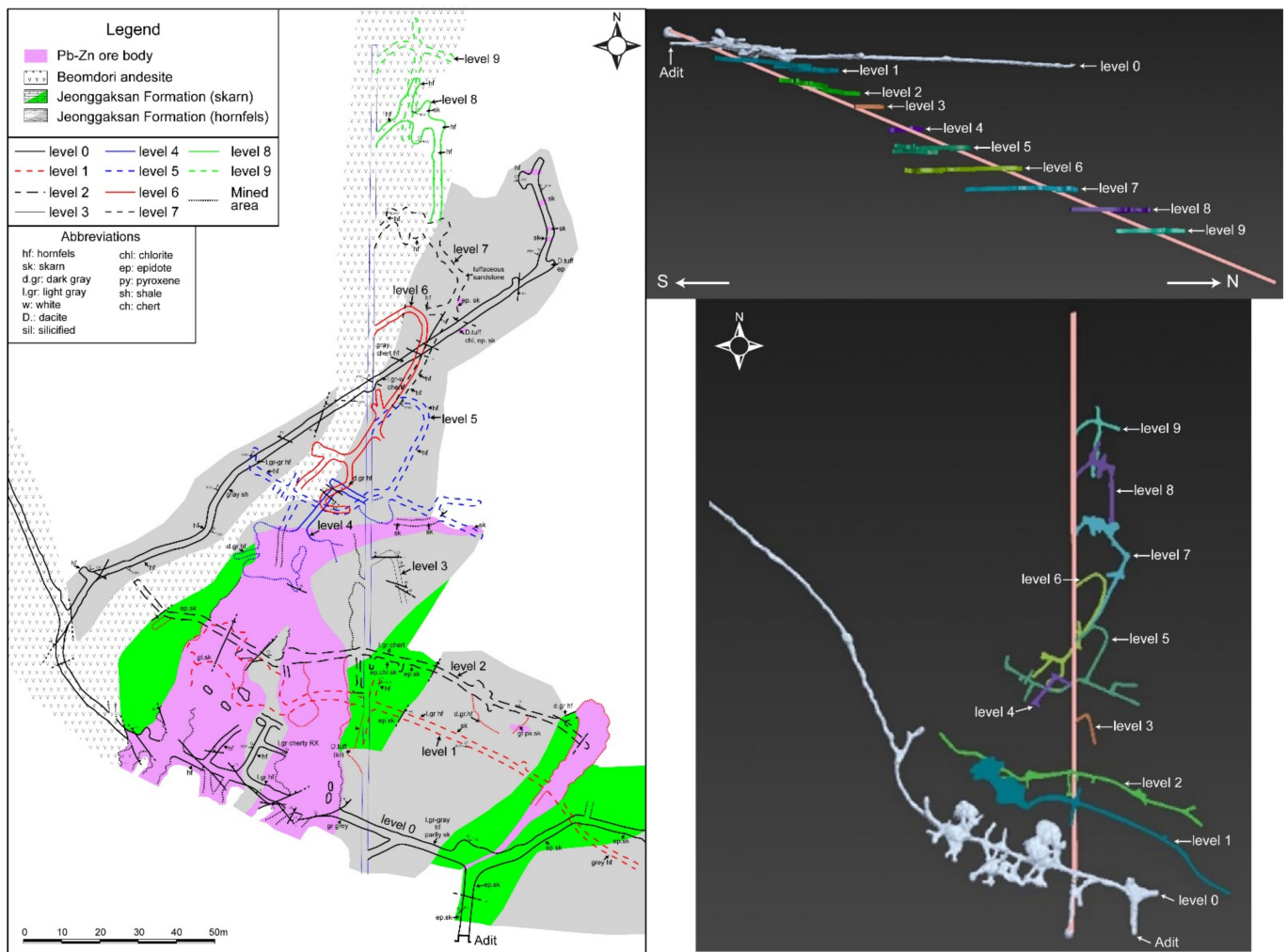


Figure 13. Microphotographs of the chloritized epidote skarn. (A) Fracture-filling chlorite (Ch) in the amphibole skarn. (B) Chlorite layering.

6. Skarn Mineralization

6.1. Orebody Geometry

The geology of the underground mining level is composed of hornfelsic rock, andesitic tuff, skarn rocks, and Pb–Zn orebody belonging to the Jeonggaksan Formation and Beomdori andesite (Figure 14). The Beomdori andesite shows a fault contact with epidote skarn of the Jeonggaksan Formation. Most hornfelsic rocks preserve the original structures, such as lamination and bedding. The orebody is distributed concordantly with the bedding (NW strike and NE dip) of the Jeonggaksan Formation and is surrounded by hornfelsic rock and epidote-skarn (Figure 14). The mineralization would have been caused within the limestone beds, selectively and limitedly, along the bedding and fracture zones. The shape of the orebody identified in the underground mining level of the deposit seems to be of a disk- or plate-type, with a convex form at the center. It was characterized as a geometric shape with a wide width in the south and a narrow edge in the north and it shows a NW strike and a gentle NE dip (Figure 14). This disk-type orebody would be formed, limitedly and selectively, due to structural control throughout the vertical rise and lateral migration of the hydrothermal fluids derived from the concealed related intrusive.



6.2. Mineralization

Skarn ore minerals are mainly composed of sphalerite, chalcopyrite, galena, arsenopyrite, and pyrite. Ore minerals occur commonly as fracture filling and rarely disseminated minerals, and also in veinlets. Fracture-filling is the most common characteristic. The dominant mineral assemblages are sphalerite–chalcopyrite–galena (–arsenopyrite), sphalerite–galena–chalcopyrite–pyrite, and sphalerite–galena–pyrite (–arsenopyrite). Sphalerite, the major skarn mineral, occurs as a large irregular crystal or an aggregate and fills the fractures in the cataclastic matrix. It commonly contains small grains of chalcopyrite and irregular galena (Figure 15A,B). Chalcopyrite characteristically occurs as an inclusion within sphalerite (Figure 15A). The intergrowth of chalcopyrite blebs within sphalerite—termed “chalcopyrite disease”, first introduced by [22]—is a common and characteristic occurrence in the deposit. Pyrite is the second dominant sulfide mineral, occurring as large euhedral single grains and small anhedral/subhedral aggregates. It has commonly replaced the sphalerite and filled the fractures of fragmented sphalerite (Figure 15C). Pyrite has also been replaced by sphalerite (Figure 15D). Therefore, pyrite seems to have formed before and after sphalerite. This indicates that the pyrite was precipitated throughout all skarn stages. Galena occurs as an inclusion within the sphalerite (Figure 15A,B) and commonly replaced sphalerite (Figure 15E,F). It also replaces pyrite (Figure 15G). Arsenopyrite showing a wedge shape occurs rarely and contains sphalerite inclusions (Figure 15H) and, therefore, seems to have formed after sphalerite. The paragenetic sequence of the major skarn

sulfide minerals in the deposit is thought to be fine anhedral/subhedral pyrite, sphalerite, chalcopyrite, galena, and large euhedral pyrite.

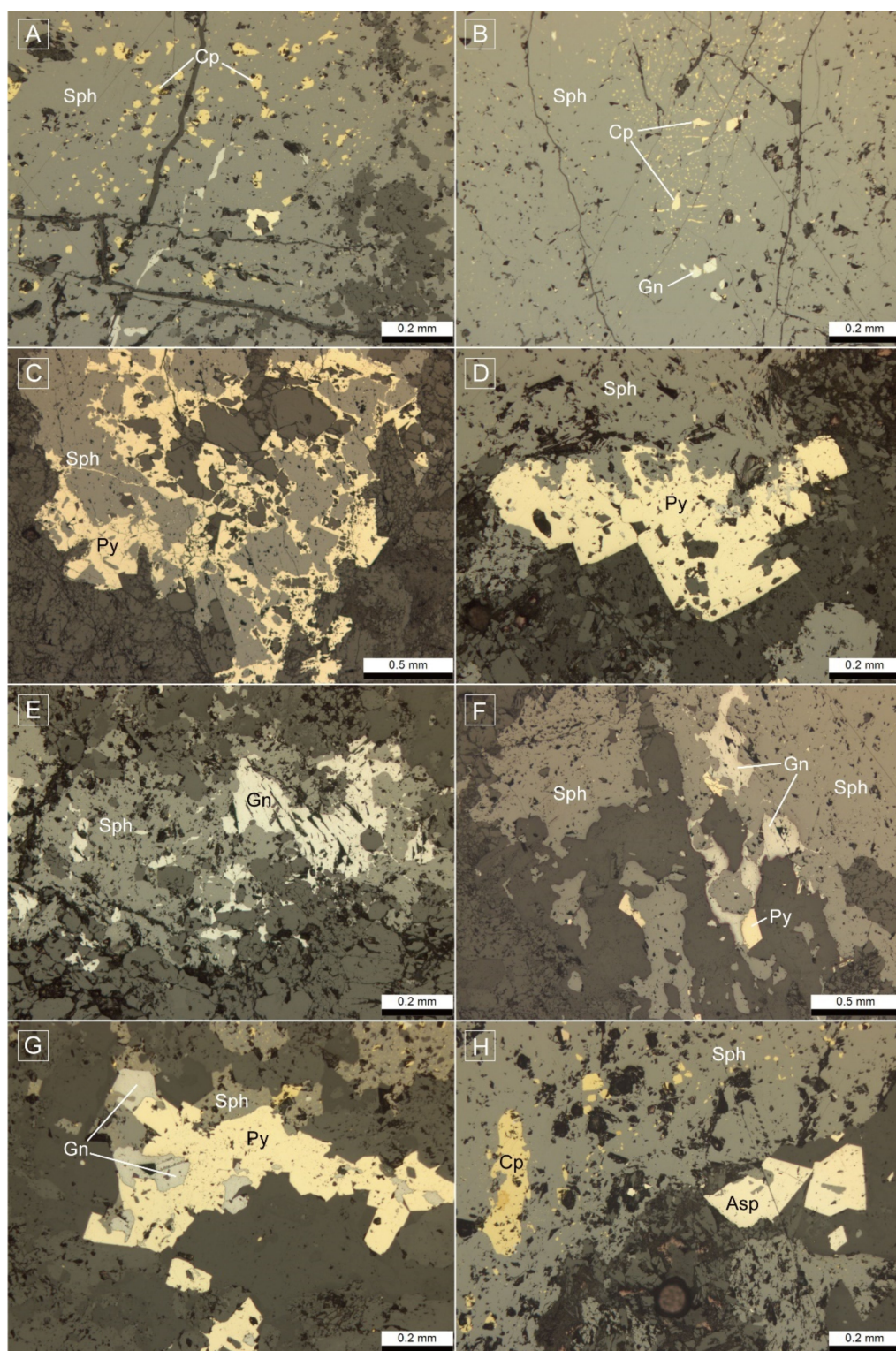


Figure 15. Microphotographs under reflected microscope. (A,B) Chalcopyrite (Cp) and galena (Gn) inclusions within sphalerite (Sph). (C,D) Pyrite (Py) replaces sphalerite. (E,F) Galena replaces sphalerite. (G) Galena replaces pyrite. (H) Arsenopyrite (Asp) is associated with sphalerite.

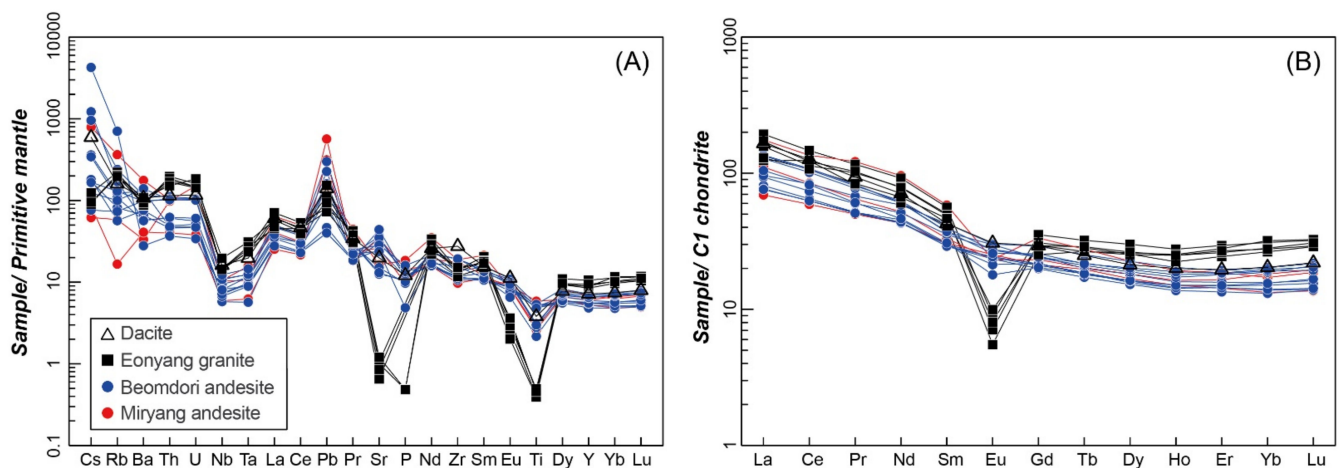


Figure 17. (A) Trace element spider diagram (primitive values from [25]); (B) C1 chondrite [25] normalized REE patterns.

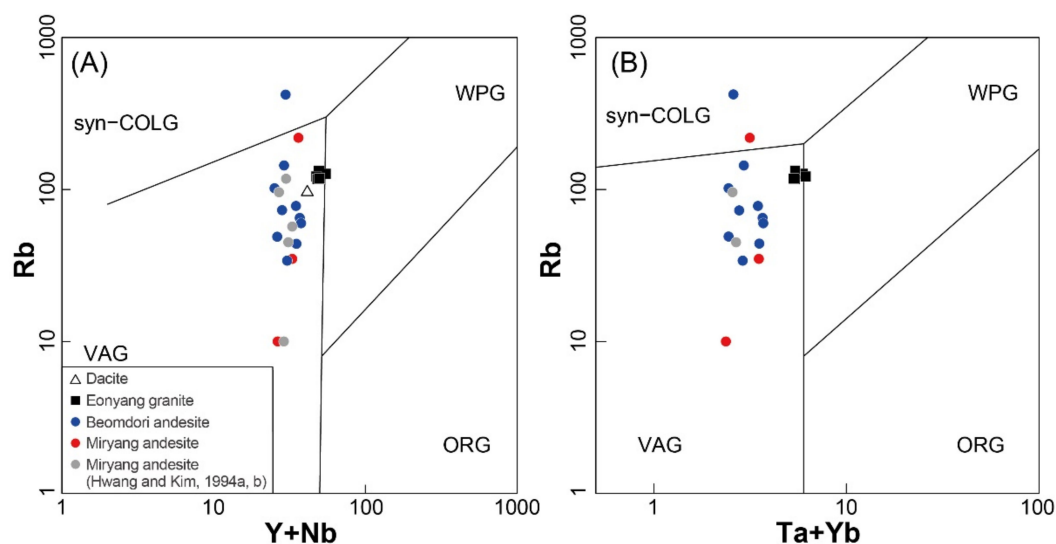


Figure 18. Tectonic discrimination diagrams with discrimination fields after [26] for the analyzed samples. (A) Rb-(Y+Nb) diagram; (B) Rb-(Ta+Yb) diagram. Abbreviations: syn-COLG, syn-collisional granites; VAG, volcanic arc granites; WPG, within-plate granites; ORG, ocean-ridge granites.

7.2. Boron, Lead, and Zinc Geochemistry

As mentioned above, axinite is the most important skarn mineral in the Gukjeon Pb–Zn deposit. Axinite in this deposit is closely related to the Pb–Zn ore minerals. Axinite can have a much higher boron (B_2O_3) content than other skarn minerals (pyroxene, garnet, amphibole, and epidote). Boron is a lithophile element, commonly occurring as a minor component in granite melt, while a total B_2O_3 concentration of about 1 wt.% can be reached in highly evolved peraluminous tourmaline-bearing granite [27]. It also can be easily transported during the fluid–rock interaction and has significance for tracing the fluid source in hydrothermal ore deposits [28].

To trace the source of the boron, we checked the boron contents of the fresh volcanic and igneous rocks neighboring the Gukjeon Pb–Zn deposit. We further analyzed the boron contents of Beomdori andesite-hosted argillic altered rocks in the southern and eastern sides of the Gukjeon deposit to compare the fluid sources of the skarn Pb–Zn mineralization in the Gukjeon deposit and the argillic alteration near the deposit.

The altered andesitic rocks from the Miryang and Jeonggaksan andesites have anomalous high boron contents (11.4 ppm and 82.6 ppm for Jeonggaksan andesite and 28.3 to 370 ppm for Miryang andesite). Argillic altered rocks including pyrophyllite and kaolin

have moderately anomalous boron contents, ranging from 0.9 to 44.3 ppm (Table 1). Both fine-grained granodiorite and Eonyang granite have relatively low boron contents of 5.3 and 6.9 ppm for the fine-grained granodiorite and 0.6 to 5.4 ppm for the Eonyang granite (Table 1). Considering the boron contents, the altered andesitic rocks of the Jeonggaksan Formation and Miryang andesite, as well as the axinite skarn in the deposit, would be affected by boron-bearing fluid. Therefore, a boron-rich fluid probably affected the argillic alteration of the Beomdori andesite as well as the skarn alteration in the deposit. The granitoids such as fine-grained granodiorite and Eonyang granite can be excluded from the boron source due to their low boron concentrations.

Table 1. Boron, lead, and zinc contents (ppm) of the altered rocks and neighboring granitoids near the Gukjeon Pb–Zn deposit.

Unit	Sample No.	B	Pb	Zn	Unit	Sample No.	B	Pb	Zn
Jeonggaksan andesite	20KJ-2-1	11.4	35	50		20KJ-8	0.9	23	n.d.
	20KJ-2-2	82.6	13	40		20KJ-9	5.1	37	n.d.
Andesitic rocks (Miryang andesite)	19KJ18-1	122	85	360	Argillic altered rocks (Beomdori andesite-hosted)	20KJ-10-1	34.3	48	n.d.
	210105-1-1	370	75	30		20KJ-10-2	10.5	13	n.d.
	210105-2-1	160	120	40		20KJ-10-3	27.7	65	n.d.
	210105-2-2	28.3	n.d.	n.d.		20KJ-10-4	44.3	20	60
	210105-3	123	223	460		20KJ-10-5	33	14	n.d.
	210105-4	87	105	660	Fine-grained granodiorite	20KJ-16	6.9	11	80
210105-5	54.5	119	670	20KJ-17		5.3	10	80	
Andesitic rocks (Beomdori andesite)	20KJ-3	9.3	7	80	Granitic rocks (Eonyang granite)	19KJ-1008	5.4	12	40
	20KJ-4a	6.4	13	100		19KJ-1009	1	17	60
	20KJ-4b	12.3	24	110		19KJ-1010	0.6	11	50
	20KJ-5	13.5	24	180		19KJ-1011	2.8	14	60
	20KJ-7	9.7	6	140		19KJ-1012	1.4	23	80

n.d. not detected.

8. Zircon SHRIMP U–Pb Geochronology

The representative CL images and SHRIMP U–Pb results are listed in Figure 19 and Table S7, respectively. Two andesitic lavas (19KJ-20 and 19KJ-18) and one andesite porphyry (19KJ-18-1) from the Miryang Andesite were selected for the SHRIMP zircon U–Pb analyses. Zircon grains from the andesitic lava (19KJ-20) are equant to prismatic and euhedral crystals with oscillatory or banded zoning in CL images (Figure 19). The U and Th contents range from 62 to 308 ppm and 56 to 280 ppm, respectively (Table S7). Th/U ratios vary from 0.66 to 1.09. The weighted mean age of the analyzed points yields 93.1 ± 1.3 Ma ($n = 12$, MSWD = 1.4; Figure 20). Zircons from the andesitic lava (19KJ-18) are generally euhedral prismatic grains with oscillatory, banded, or sector zoning (Figure 20). The ranges of U content (78–393 ppm), Th content (41–443 ppm), and Th/U ratios (0.38–1.14) are very similar to those of the 19KJ-20. The weighted mean age yields 91.0 ± 1.2 Ma ($n = 16$, MSWD = 2.8; Figure 20). Zircon crystals from the andesitic porphyry (19KJ-18-1) are euhedral prismatic or equant grains, showing oscillatory, banded, or sector zoning (Figure 20). The U (64–547 ppm) content, Th (21–477 ppm) content, and Th/U ratio (0.33–0.87) are very similar to those of the two andesitic lavas. The weighted mean age from this sample is 90.1 ± 1.4 Ma ($n = 18$, MSWD = 3.5). Considering the CL texture and Th/U ratios, the eruption ages are interpreted as 93 to 91 Ma for the andesitic lava and 90.1 Ma for the andesite porphyry.



Figure 19. Representative CL images of the analyzed zircons. Red ellipses are analyzed points; their lengths are 30 μm . The numbers are ^{207}Pb corrected $^{206}\text{Pb}/^{238}\text{U}$ ages.

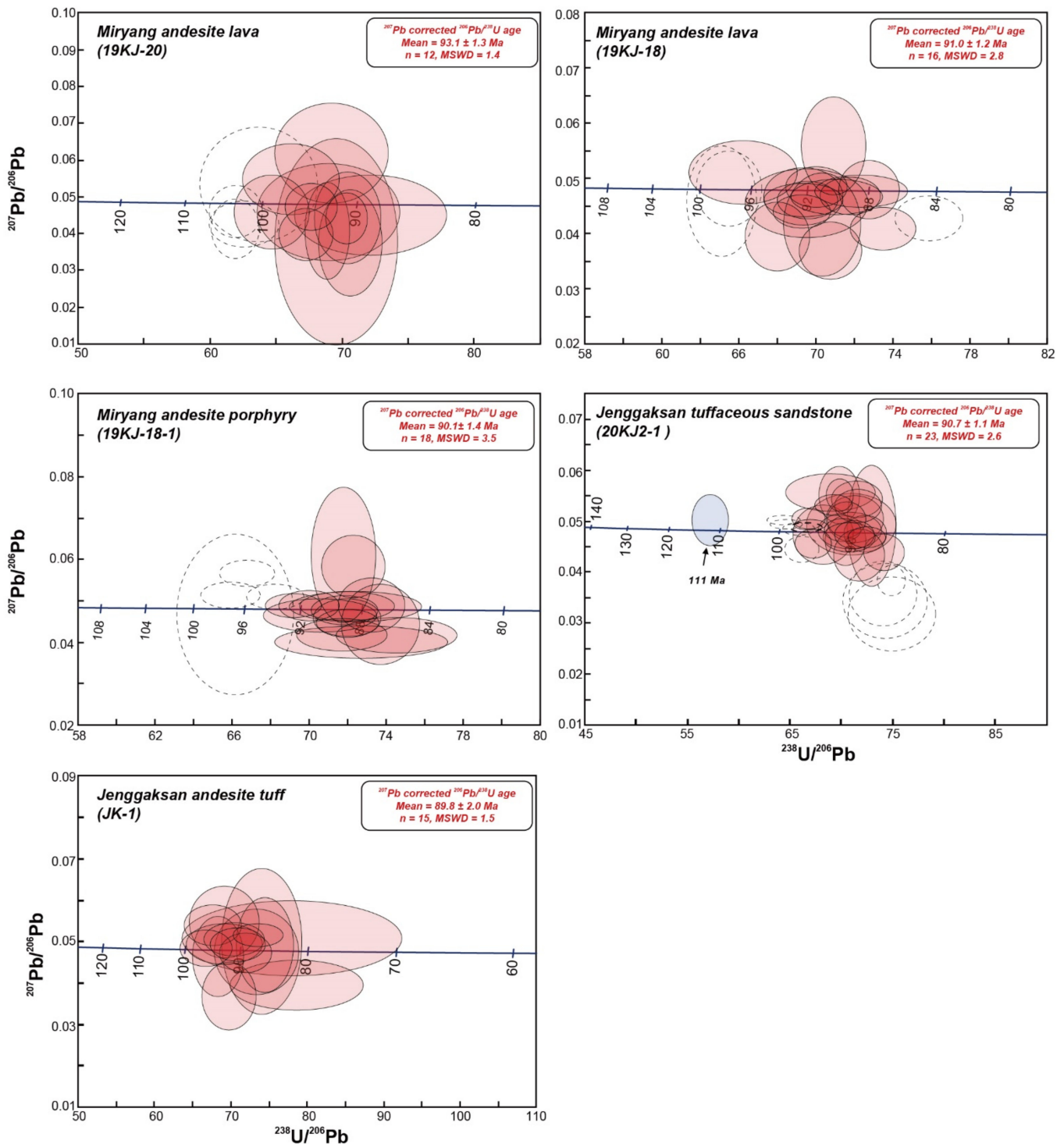


Figure 20. Terra–Wasserburg diagrams for the Miryang andesitic rocks (19KJ-20, 19KJ-18, and 19KJ-18-1), Jeonggaksan tuffaceous sandstone (20KJ2-1), and Jeonggaksan andesite tuff (JK-1). Dashed ellipses are the rejected data by weighted mean age calculation.

Two samples were selected from the Jeonggaksan Formation (20KJ2-1 and JK-1). Zircon grains from the tuffaceous sandstone (20KJ2-1) are generally prismatic crystals with oscillatory zoning (Figure 19). Their U and Th contents range from 55 to 5958 ppm and 20 to 2860 ppm, respectively. Their Th/U ratios vary from 0.25 to 0.92. One of these grains has an unzoned dark-CL emission of the inherited core, yielding an apparent age of 111.4 Ma.

Except for one datum, the analyzed data form one cluster and yield a weighted mean age of 90.7 ± 1.1 Ma ($n = 23$, MSWD = 2.6; Figure 20), which is interpreted as the maximum depositional age for the tuffaceous sandstone. Zircons from the andesite tuff (JK-1) are euhedral and stubby prisms with typical oscillatory zoning (Figure 19). The weighted mean age from all the analyzed data yields 89.8 ± 2.0 Ma ($n = 15$, MSWD = 1.5; Figure 20), which is the eruption age of the andesite tuff.

We selected three porphyritic andesites (19KJ-22, JK-4, and JK-6) and one andesitic tuff (JK-3) from the Beomdori andesite for SHRIMP zircon U–Pb age dating. Zircon grains from the porphyritic andesite (19KJ-22) are generally euhedral grains with banded or oscillatory zoning (Figure 19). One data point (point 10.1) yields 155.1 ± 3 Ma, interpreted as the inherited core of this porphyritic andesite. The rest of the analyzed data points yield a weighted mean age of 84.88 ± 0.94 Ma ($n = 26$, MSWD = 2.8; Figure 21). The U and Th concentrations range from 103 to 520 ppm and 61 to 633 ppm, respectively. Their Th/U ratios vary from 0.59 to 1.28. Zircon crystals from the porphyritic andesite (JK-6) are generally euhedral, prismatic grains showing a banded, combining sector, and oscillatory zoning (Figure 19). The analyzed data points yield a weighted mean age of 83.8 ± 1.6 Ma ($n = 14$, MSWD = 1.3; Figure 21). Their U and Th contents and Th/U ratios range from 57 to 1348 ppm, 38 to 1421 ppm, and 0.51 to 1.31 ppm, respectively. Zircons from the porphyritic andesite (JK-4) are very similar to those of the previous two porphyritic andesites (19KJ-22 and JK-6). All the analyzed data points make one cluster on the Terra–Wasserburg diagram and yield a weighted mean age of 83.8 ± 1.3 Ma ($n = 16$, MSWD = 1.03; Figure 21). The U content (81–436 ppm), Th content (49–546 ppm), and Th/U ratios (0.60–1.36) are also in a very similar range to those of samples 19KJ-22 and JK-6. Considering all analyzed data from the three porphyritic andesites of the Beomdori andesite (19KJ-22, JK-6, and JK-4), the porphyritic andesites appear to have erupted between 88.88 and 83.8 Ma. Zircon crystals from the andesitic tuff (JK-3) are euhedral, prismatic grains generally showing combined oscillatory and sector zoning (Figure 19). Their U and Th contents range from 85 to 654 ppm and 58 to 1075 ppm, respectively. Their Th/U ratios vary from 0.54 to 1.64. All analyzed data form one cluster in the Terra–Wasserburg diagram and yield a weighted mean age of 81.1 ± 1.1 Ma ($n = 18$, MSWD = 1.02; Figure 21), which was interpreted as the eruption age of the andesitic tuff.

Zircon grains from two samples (20KJ-16 & 20KJ-17) of fine-grained granodiorite show a similar CL texture. Those zircons are prismatic to hexagonal grains with an oscillatory or banded texture. The U and Th contents and Th/U ratios from sample 20KJ-16 range from 130 to 686 ppm, 96 to 1094 ppm, and 0.74 to 1.62, respectively, while those for sample 20KJ-17 vary between 85 and 831 ppm, 62 and 1564 ppm, and 0.58 and 1.88, respectively. The weighted mean ages for the two samples are 82.79 ± 1.80 Ma ($n = 35$, MSWD = 2.5) and 81.64 ± 0.41 Ma ($n = 38$, MSWD = 1.6). Together with the CL texture and Th/U ratios, fine-grained granodiorite intruded around 82 Ma (Figure 21).

Zircons from the granitic rock of the Eonyang granite (19KJ-1012) are euhedral, prismatic grains with oscillatory zoning (Figure 19). All of the analyzed data form one cluster on the Terra–Wasserburg diagram and yield 72.0 ± 1.0 Ma ($n = 22$, MSWD = 1.5; Figure 21). Their U and Th contents and Th/U ratios range from 202 to 1158 ppm, 104 to 866 ppm, and 0.49 to 1.39, respectively. Considering their CL texture and Th/U ratios, Eonyang granite intruded at 72.0 Ma.

Zircon grains from dacite (19KJ-1001) are equant to prismatic crystals showing oscillatory, patch, and sector zoning (Figure 19). Their weighted mean age is calculated as 68.62 ± 0.93 Ma ($n = 15$, MSWD = 0.97; Figure 21). Their U and Th contents and Th/U ratios vary from 37 to 940 ppm, 45 to 1822 ppm, and 0.49 to 2.29, respectively. Considering zircon texture and Th/U ratios, dacite erupted at 68.62 Ma.

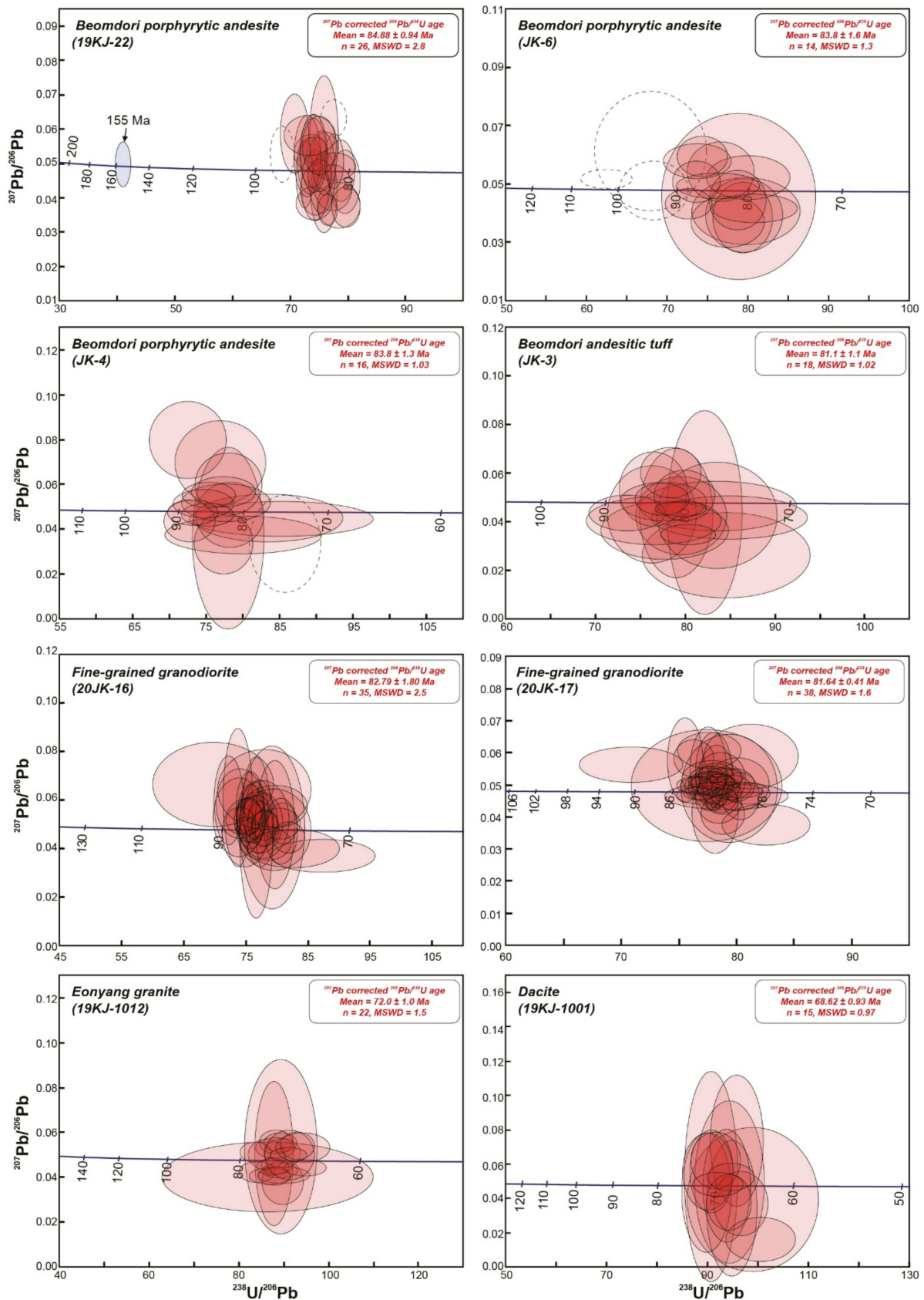


Figure 21. Terra–Wasserburg diagrams for the Beomdori andesitic rocks (19KJ-22, JK-6, JK-4, and JK-3), fine-grained granodiorite (20JK-16, 20JK-17), Eonyang granite (19KJ-1002), and dacite (19KJ-1001). Dashed ellipses are the rejected data by the weighted mean age calculation.

We integrated the age dating results with the previous geochronological study [29]. The volcanism and sedimentation occurred as the successive stages or pulses, forming the Milyang andesite from 94.3 to 93.1 Ma, the Jeonggaksan Formation (andesite, andesitic tuff and tuffaceous sedimentary rocks) from 91.0 to 88.7 Ma, the Beomdori andesite from 84.9 to 78.4 Ma, and dacite and granite (Eonyang granite) from 72.0 to 68.6 Ma in the study area (Table 2 and Figure 22). The Jeonggaksan Formation, which was formed under submarine and subaerial environments, including carbonate beds, is the host formation of the Gukjeon Pb–Zn deposit (Figure 22). Based on the age dating results and field occurrences, we suggest a simplified model showing the geological events including the mineralization (Figure 22).

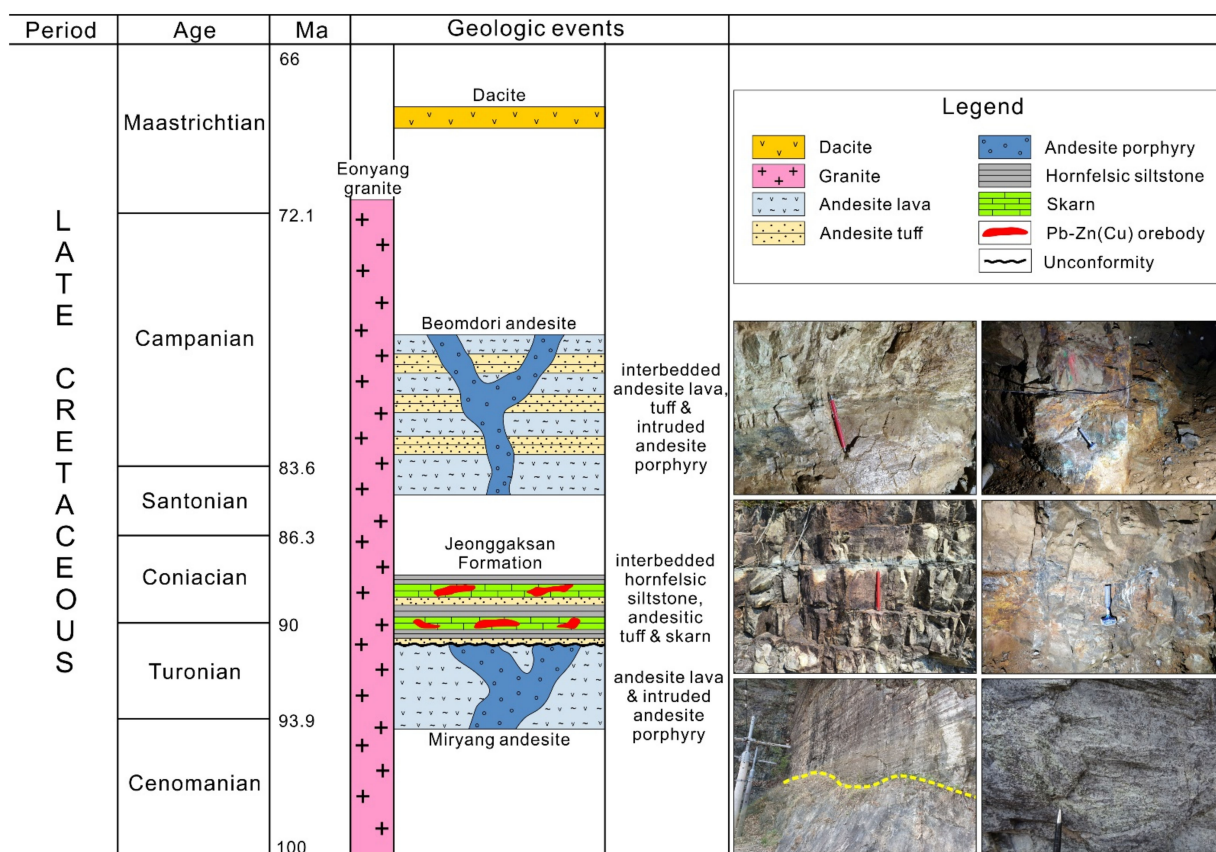


Figure 22. Simplified lithological sequence based on the geochronology of the study area.

Table 2. SHRIMP and SIMS zircon age dating results for the igneous rocks of the study area.

Formation or Igneous Body	Sample Number	Rock Type	Dating Method	Age (Ma)	Reference
Dacite	19KJ-1001	dacite		68.6 ± 0.9	
Eonyang granite	19KJ-1012	granite		72.0 ± 1.0	
Fine-grained granodiorite	20JK-16	granodiorite	SHRIMP	82.8 ± 1.8	This study
	20JK-17	granodiorite		81.6 ± 0.4	
Beomdori andesite	JK-3	andesitic tuff		81.1 ± 1.1	
	JK-4	porphyritic andesite		83.8 ± 1.3	
	JK-6		83.8 ± 1.6		
	19KJ-22		84.9 ± 0.9		
	090615-8	andesite	IMS-1280	78.4 ± 1.5	[29]

Table 2. Cont.

Formation or Igneous Body	Sample Number	Rock Type	Dating Method	Age (Ma)	Reference
Jeonggaksan Formation	JK-1	andesitic tuff	SHRIMP	89.8 ± 2.0	This study
	20KJ2-1	tuffaceous sandstone		90.7 ± 1.1	
	090616-15	tuff	IMS-1280	88.7 ± 0.7	[29]
	090616-1	andesite		88.8 ± 1.0	
Miryang andesite	19KJ-18-1	andesite porphyry	SHRIMP	90.1 ± 1.4	This study
	19KJ-18	andesite lava		91.0 ± 1.2	
	19KJ-20	andesite lava		93.1 ± 1.3	
	090615-3	andesite	IMS-1280	94.3 ± 2.0	[29]

9. Discussion and Conclusions

Skarn formation was restricted to the limestone member of the Jeonggaksan Formation, where the major skarn minerals are garnet (mainly grossular with minor andradite), hedenbergite, amphibole (actinolite and ferro-actinolite), axinite (tizenite and ferroaxinite), and epidote (clinozoisite and epidote). The most characteristic skarn mineral was abundantly occurring axinite, which can be formed under a plentiful supply of boron derived from magma or a hydrothermal solution. Boron content is a good indicator for understanding the magmatic–hydrothermal evolutionary processes forming metallic deposits [30]. The occurrence of abundant axinite in the deposit indicates the continuous boron supply from the hydrothermal system forming the deposit. Skarn alteration in the deposit is characterized by prograde metasomatic pyroxene and garnet and retrograde metasomatic amphibole, axinite, and epidote. In the final stage, weak chloritization and silicification after the skarnization occurred in the deposit. The sequence of the skarn and alteration minerals in the deposit was interpreted as being in the order of pyroxene → garnet → amphibole → axinite → epidote → chlorite throughout the metasomatic and hydrothermal processes in the system. The major skarn sulfide minerals of sphalerite, chalcopyrite, galena, and pyrite were mostly deposited during the retrograde stage which formed amphibole and axinite skarns. The major skarn sulfide minerals would have been formed in the order of small anhedral/subhedral pyrite, sphalerite, chalcopyrite, galena, and large euhedral pyrite. The chalcopyrite disease texture, with the inclusion of chalcopyrite blebs within sphalerite, can be explained by the selective dissolution of Fe-rich sphalerite and the addition of Cu (or both Cu and Fe) from fluid sources [31] or sphalerite–chalcopyrite co-precipitation by exsolution [32,33].

The Jeonggaksan Formation was formed from the Turonian to the Coniacian. The andesite (sample 090615-8, 78.4 ± 1.5 Ma, MSWD = 1.0, $n = 3$) from Beomdori andesite [29] is distinct from our results (porphyritic andesite, 84.9 ± 0.9 , 83.8 ± 1.6 , and 83.8 ± 1.3 Ma; andesitic tuff, 81.1 ± 1.1 Ma). In addition, the authors of [29] did not report detailed information for the analyzed Beomdori andesite such as petrography and geochemistry. Furthermore, the authors of [34] pointed out that the age dating results in [29] for Beomdori andesite were not matched to the lithological sequence of the neighboring area. We therefore suggest that the exact extrusion or intrusion age for the Beomdori andesitic rocks should be circa 84.9 to 83.8 Ma. The Eonyang granite intruded the Jusasan and Unmunsa subgroups and the emplacement age is 72.0 ± 1.1 Ma. This emplacement age is coincident with the crystallization ages ([29]; 71.1 ± 0.8 , 72.4 ± 0.6 , 72.4 ± 0.7 , and 71.8 ± 0.6 Ma) within the uncertainties. The final volcanic eruption recorded in the dacite (68.6 ± 0.9 Ma) in the study area occurs in the Maastrichtian.

As mentioned above, the occurrence of axinite, a major boron-bearing mineral, gives an important clue to understanding the skarn mineralization. The andesitic rocks from the

Miryang andesite and Jeonggaksan Formation show geochemical affinities for B–Pb–Zn by the participation of boron-rich ore-bearing fluid in the system (Figure 23). This probably indicates that the Pb–Zn mineralization in the deposit was coeval with formation of the axinite skarn. Boron is a major component of the ore-bearing fluid in the study area. Despite the absence of age dating results for the ore minerals, the timing of mineralization could be constrained by boron-rich hidden magmatic rocks during late Cretaceous (Campanian) (Figure 23). These results are different from the conclusions for the skarn mineralization associated with the Bulguksa granitoids (e.g., Eonyang granite) suggested by previous studies [6,7] and implicate hidden sources under the current surface level.

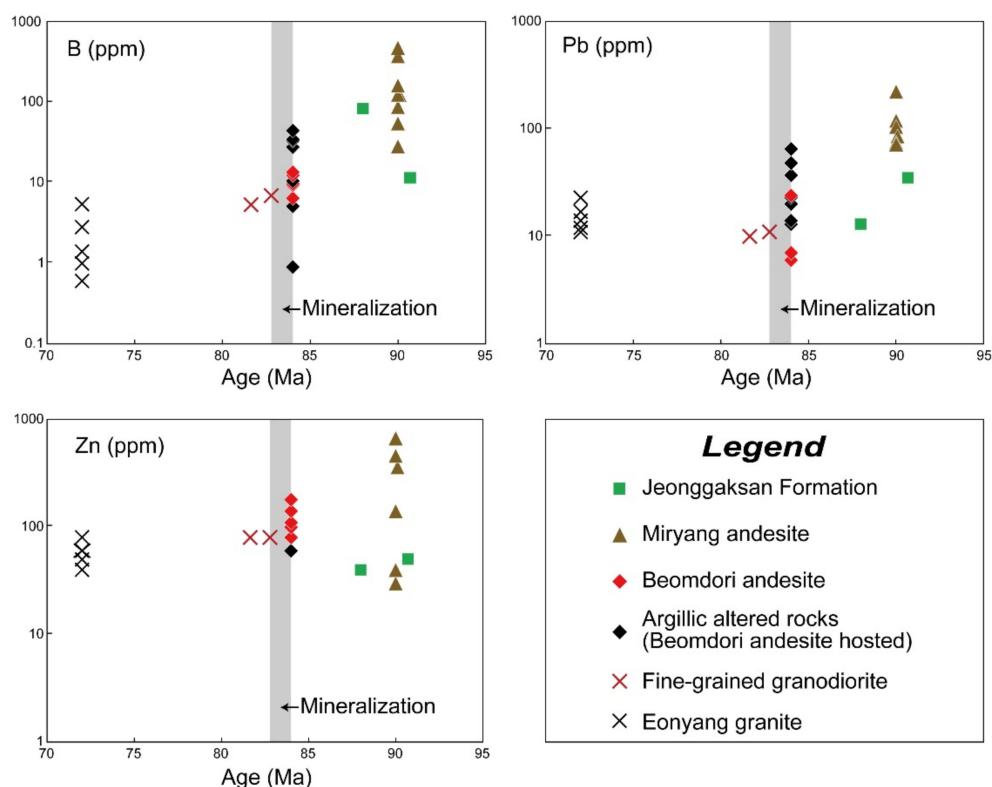


Figure 23. Age vs. B, Pb, and Zn diagrams for the altered rocks and neighboring granitoids of the Gukjeon Pb–Zn deposits.

The skarn alteration zone occurs in the limestone horizon in the Jeonggaksan Formation and the skarnization processes can be divided into prograde, retrograde, and final chloritization and silicification stages. The occurrence of axinite in the axinite skarn gives an important clue to the participation of boron-rich fluid in the skarn alteration and related mineralization. Concluding from the boron contents and geochronological results for the neighboring magmatic rocks, the ore minerals of the Gukjeon Pb–Zn deposit were probably precipitated by the infiltration and migration of boron-rich fluids derived from hidden pluton in the Campanian of the Late Cretaceous.

Supplementary Materials: The following are available online at <https://www.mdpi.com/article/10.3390/min11060619/s1>. Figure S1: Rock slabs (A and B) and microphotographs (B and D) of andesitic rocks from the Miryang andesite. A and B are andesite lava with small plagioclase lath and small epidotized pyroxene (Ep) phenocrysts, which show a trachytic texture. C and D are porphyritic andesites consisting of phenocrysts of zonal plagioclase (Pl), pyroxene (Px), and glassy groundmass. Figure S2: Outcrops (A and B), rock slabs (C and E), and microphotographs (D and F) of the Jeonggaksan Formation. A: Unconformity between the Jeonggaksan Formation in the upper part and the Miryang andesite in the lower part; B: Interbedded limestone within the Jeonggaksan Formation; C: Weakly bedded tuffaceous sandstone of the Jeonggaksan Formation; D:

Microphotographs of the rock slab in C; E: Andesitic tuff interbedded with tuffaceous sediments; F: Microphotographs of the rock slab in E. RF, Rock fragment; Ep, Epidote. Figure S3: Rock slabs (A, C, and E) and microphotographs (B, D, and F). A and B: Beomdori andesite; C and D: Dacite; E and F: Eonyang Granite. Bt, Biotite; Pl, Plagioclase; VQ, Vermicular quartz. Table S1: Chemical compositions of major and trace elements of igneous rocks near Gukjeon Pb–Zn deposit. Table S2: SHRIMP zircon U–Th–Pb isotope data of the study area. Table S3: EPMA analytical results for pyroxene. Table S4: EPMA analytical results for garnet. Table S5: EPMA analytical results for amphibole. Table S6: EPMA analytical results for axinite. Table S7: EPMA analytical results for epidote.

Author Contributions: N.K., S.-M.K., B.-W.Y., and B.H.L. designed and participated in the research. All authors are responsible for the field geologic survey as well as the petrological, mineralogical, and geochemical analyses. All authors have read and agreed to the published version of the manuscript.

Funding: This work was supported by the National Research Council of Science & Technology (NST) grant of the Korean government (MSIT) (No.CRC-15-6- KIGAM).

Data Availability Statement: All data are contained within the article and Supplementary Figures and Tables.

Acknowledgments: We are grateful to Jaehyung Yu and Changhyeok Park for their assistance with 3D laser scanning and creating the 3D underground map. Insightful comments by the academic editor, Chris Brown, and two anonymous reviewers have greatly improved the manuscript. This work was supported by the National Research Council of Science & Technology (NST) grant by the Korea government (MSIT) (No.CRC-15-06-KAGAM).

Conflicts of Interest: The authors declare no conflict of interest.

References

- Kim, T. *Technical Report of Gukjeon Mine. KORES Report*; KORES: Wonju, Korea, 1999; p. 10. (In Korean)
- Kang, H. *Korea Resources Corporation. Reports on Drilling Results of Gukjeon Pb-Zn Mine*; KORES: Wonju, Korea, 2009; p. 13. (In Korean)
- Choi, D.; Hwang, H.; Oh, G.; Jeong, D. *KORES. Report on Detailed Survey Result (Mo: Sangju Area) (Zn-Pb: Samcheok and Miryang area) (Cu: Jeongsun Area), DS2012-MT(III), (IV), (V)*; KORES: Wonju, Korea, 2012; p. 80. (In Korean)
- Sung, J. *Report on 2013 Drilling Results of Gukjeon Pb-Zn Mine. KORES Report*; KORES: Wonju, Korea, 2014; p. 19. (In Korean)
- Yang, C.; Choi, J.B. Occurrence of the Pb–Zn Skarn Deposits in Gukjeon Mine, Korea. *J. Mineral. Soc. Korea* **2010**, *23*, 413–428. (In Korean with English Abstract)
- Kwak, J.Y.; Kang, C.W.; Joo, S.Y.; Jeong, J.H.; Choi, J.B. Occurrence of Zn–Pb Deposits in Danjang-Myeon, Milyang Area. *J. Mineral. Soc. Korea* **2015**, *28*, 279–292. [[CrossRef](#)]
- Ryu, I.-C.; Choi, S.-G.; Wee, S.-M. An Inquiry into the Formation and Deformation of the Cretaceous Gyeongsang (Kyongsang) Basin, Southeastern Korea. *Econ. Environ. Geol.* **2006**, *39*, 129–149. (In Korean with English Abstract)
- Koh, S.-M.; Ryoo, C.-R.; Song, M.-S. Mineralization Characteristics and Structural Controls of Hydrothermal Deposits in the Gyeongsang Basin, South Korea. *Resour. Geol.* **2003**, *53*, 175–192. [[CrossRef](#)]
- Chae, U.; Kim, G.; Hong, S.; Lee, B.; Hwang, J.; Park, K.; Hwang, S.; Choi, B.; Song, G.; Jin, M. *Geological Map of Korea (1:1,000,000)*. Korea Institute of Geology, Mining and Materials, 1995. (In Korean with English Abstract)
- Kim, K.B.; Hwang, S.K. *Geological Report of The Miryang Sheet (SCALE 1:50,000)*; Korea Institute of Energy and Resources: Seoul, Korea, 1988. (In Korean with English Abstract)
- Hong, S.H.; Choi, P. *Geological Report of the Yucheon Sheet*; Korea Institute of Energy and Resources: Seoul, Korea, 1988. (In Korean with English Abstract)
- Takagi, T.; Koh, S.; Kim, M.; Naito, K.; Sudo, S. Geology and Hydrothermal Alteration of the Milyang Pyrophyllite Deposit, Southeast Korea. *Resour. Geol.* **2000**, *50*, 243–256. [[CrossRef](#)]
- Koh, S.-M.; Takagi, T.; Kim, M.; Naito, K.; Hong, S.; Sudo, S. Geological and Geochemical Characteristics of the Hydrothermal Clay Alteration in South Korea. *Resour. Geol.* **2000**, *50*, 229–242. [[CrossRef](#)]
- Paces, J.B.; Miller, J.D., Jr. Precise U–Pb ages of Duluth Complex and related mafic intrusions, Northeastern Minnesota: Geochronological insights to physical, petrogenic, paleomagnetic, and tectonomagmatic processes associated with the 1.1 Ga midcontinent rift system. *J. Geophys. Res.* **1993**, *98*, 13997–14013. [[CrossRef](#)]
- Williams, I.S. U–Th–Pb geochronology by ion microprobe. In *Applications of Microanalytical Techniques to Understanding Mineralizing Processes*; Reviews in Economic Geology; McKibben, M.A., Shanks, W.C., III, Rindley, W.I., Eds.; Society of Economic Geologists: Littleton, CO, USA, 1998; Volume 7, pp. 1–35.
- Ludwig, K.R. *User's Manual for Isoplot 3.7 A Geochronological Toolkit for Microsoft Excel*; Berkeley Geochronological Center: Berkeley, ON, Canada, 2008.
- Morimoto, N. Nomenclature of Pyroxenes. *Mineral. Petrol.* **1988**, *39*, 55–76. [[CrossRef](#)]

18. Mange, M.A.; Morton, A.C. Chapter 13 Geochemistry of Heavy Minerals. In *Developments in Sedimentology*; Elsevier: Amsterdam, The Netherlands, 2007; Volume 58, pp. 345–391. ISBN 9780444517531.
19. Leake, B.E.; Woolley, A.R.; Arps, C.E.S.; Birch, W.D.; Gilbert, M.C.; Grice, J.D.; Hawthorne, F.C.; Kato, A.; Kisch, H.J.; Krivovichev, V.G.; et al. Nomenclature of amphiboles: Report of the subcommittee on amphiboles of the international mineralogical association, commission on new minerals and mineral names. *Can. Mineral.* **1997**, *35*, 219–246.
20. Filip, J.; Dachs, E.; Tucek, J.; Novak, M.; Bezdicka, P. Low-temperature calorimetric and magnetic data for natural end-members of the axinite group. *Am. Mineral.* **2008**, *93*, 548–557. [[CrossRef](#)]
21. Franz, G.; Liebscher, A. Physical and Chemical Properties of the Epidote Minerals – An Introduction. *Rev. Mineral. Geochem.* **2004**, *56*, 1–82. [[CrossRef](#)]
22. Barton, P.B.J. Some Ore Textures Involving Sphalerite from the Furutobe Mine, Akita Prefecture, Japan. *Min. Geol.* **1978**, *28*, 293–300. [[CrossRef](#)]
23. Cox, K.G.; Bell, J.D.; Pankhurst, R.J. *The Interpretation of Igneous Rocks*; Springer Netherlands: Dordrecht, The Netherlands, 1979; ISBN 978-0-412-53410-2.
24. Peccerillo, A.; Taylor, S.R. Geochemistry of Eocene calc-alkaline volcanic rocks from the Kastamonu area, Northern Turkey. *Contrib. to Mineral. Petrol.* **1976**, *58*, 63–81. [[CrossRef](#)]
25. McDonough, W.F.; Sun, S.S. The composition of the Earth. *Chem. Geol.* **1995**, *120*, 223–253. [[CrossRef](#)]
26. Pearce, J.A.; Harris, N.B.W.; Tindle, A.G. Trace Element Discrimination Diagrams for the Tectonic Interpretation of Granitic Rocks. *J. Petrol.* **1984**, *25*, 956–983. [[CrossRef](#)]
27. Pichavant, M.; Manning, D. Petrogenesis of tourmaline granites and topaz granites; the contribution of experimental data. *Phys. Earth Planet. Inter.* **1984**, *35*, 31–50. [[CrossRef](#)]
28. Qiu, Y.; Zhang, R.; Chou, I.-M.; Wang, X.; Hu, W.; Zhang, W.; Lu, J.; Li, G.; Li, Z. Boron-rich ore-forming fluids in hydrothermal W-Sn deposits from South China: Insights from in situ Raman spectroscopic characterization of fluid inclusions. *Ore Geol. Rev.* **2021**, *132*, 104048. [[CrossRef](#)]
29. Zhang, Y.B.; Zhai, M.; Hou, Q.L.; Li, T.S.; Liu, F.; Hu, B. Late Cretaceous volcanic rocks and associated granites in Gyeongsang Basin, SE Korea: Their chronological ages and tectonic implications for cratonic destruction of the North China Craton. *J. Asian Earth Sci.* **2012**, *47*, 252–264. [[CrossRef](#)]
30. Thomas, R.; Heinrich, W.; Förster, H.J. The behaviour of boron in peraluminous granite-pegmatite systems and associated hydrothermal solutions: A melt and fluid inclusion study. *Contrib. Mineral. Petrol.* **2003**, *144*, 457–472. [[CrossRef](#)]
31. Bortnikov, N.S.; Genkin, A.D.; Dobrovolskaya, M.G.; Muravitskaya, G.N.; Filimonova, A.A. The nature of chalcopryrite inclusions in sphalerite; exsolution, coprecipitation, or “Disease”? *Econ. Geol.* **1992**, *87*, 1192–1193. [[CrossRef](#)]
32. Kojima, S. A Coprecipitation experiment on intimate association of sphalerite and chalcopryrite and its bearings on the genesis of Kuroko ores. *Min. Geol.* **1990**, *40*, 147–158.
33. Kojima, S.; Nagase, T.; Inoue, T. A coprecipitation experiment on the chalcopryrite disease texture involving Fe-bearing sphalerite. *J. Mineral. Petrol. Econ. Geol.* **1995**, *90*, 261–267. [[CrossRef](#)]
34. Hwang, S.K.; Kim, S.W.; Kim, S.; Ahn, U.S.; Jo, I.H.; Lee, S.J.; Kim, J.J. Chronostratigraphic implication of the Yucheon Group in Gyeongsang basin, Korea. *J. Geol. Soc. Korea* **2019**, *55*, 633–647. (In Korean with English Abstract) [[CrossRef](#)]